Direct formation of vertically coupled quantum dots in Stranski-Krastanow growth

N. N. Ledentsov,* V. A. Shchukin,* M. Grundmann, N. Kirstaedter, J. Böhrer, O. Schmidt, and D. Bimberg
Institut für Festkörperphysik, Technische Universität Berlin, Hardenbergstrasse 36, D-10623 Berlin, Germany

V. M. Ustinov, A. Yu. Egorov, A. E. Zhukov, P. S. Kop'ev, S. V. Zaitsev, N. Yu. Gordeev, and Zh. I. Alferov
A. F. Ioffe Physical-Technical Institute, Politekhnicheskaya 26, 194021, St. Petersburg, Russia

A. I. Borovkov
Technical University of St. Petersburg, Politekhnicheskaya 29, 195251, St. Petersburg, Russia

A. O. Kosogov,* S. S. Ruvimov,* P. Werner, U. Gösele, and J. Heydenreich
Max-Planck-Institut für Mikrostrukturphysik, Weinberg 2, D-06120 Halle, Germany

(Received 3 June 1996)

Alternate *short-period* GaAs-InAs deposition following InAs pyramid formation on a GaAs (100) surface leads to the creation of vertically split pyramids. This splitting is driven by the energetics of the Stranski-Krastanow growth mode. The strain energy is reduced due to the successive transfer of InAs from the buried part of the pyramid to the uncovered part. The resulting arrangement represents a laterally ordered array of nanoscale structures inserted in a GaAs matrix, where each structure is composed of several vertically merging InAs parts. Results of optical studies demonstrate the expected electronic coupling in vertical direction. Coupling is found to *decrease the radiative lifetime* and to result in low-energy shifts of the corresponding peaks in luminescence and absorption spectra. Vertically coupled quantum dots exhibit injection lasing at very low current densities. [S0163-1829(96)03136-0]

I. INTRODUCTION

There is a growing interest in spontaneous formation of ordered nanostructures in crystals. It has been shown that spinodal decomposition of unstable alloys can result in the formation of quasiperiodic structures in bulk crystals[1] and epitaxial films.[2] More recently, ordered nanostructures have been fabricated by utilizing self-ordering phenomena on crystal surfaces,[3–12] One mechanism relevant for *lattice-matched* growth is faceting[3,4] where a planar crystal surface rearranges to a periodic hill-and-valley structure in order to decrease the surface free energy.[5,6] Another class of effects is related to the formation of periodically ordered structures of surface domains,[7] e.g., of ordered arrays of monolayer-height islands in heterophase systems,[8–10] or flat multilayer islands.[11] Recently ordering effects have been revealed in Stranski-Krastanow (SK) growth which proceeds on a *lattice-mismatched* substrate via formation of *essentially three-dimensional islands*.[12–21] The authors of Refs. 16–19 have reported that coherent strained InAs islands formed by Stranski-Krastanow growth on GaAs (100) substrates after deposition of GaAs maintain their pyramidlike shape. Spontaneous ordering in size is caused by elastic relaxation due to the discontinuity of the intrinsic surface stress tensor at facet edges and by strain-induced renormalization of the surface energy of facets.[17,19] Lateral ordering is a result of repulsive interaction between islands.

Another degree of freedom is related to stacking of dots in the vertical direction. If InAs islands are completely covered with a sufficiently thick GaAs layer (~100 Å), InAs islands formed during the next deposition cycle exhibit a tendency to form vertically correlated structures.[12,21] However, as both electron and hole wave functions are effectively localized inside each quantum dot, this arrangement does not result in a modification of the basic properties of the structures, such as radiative lifetime, energy spectrum, carrier capture, and relaxation mechanisms or material gain. This fact initiated attempts to fabricate electronically coupled quantum dots.[19,22]

In this paper we report *an island shape transformation effect* in SK growth which results in spontaneous formation of laterally ordered arrays of structures composed of several vertically merging InAs parts in a GaAs matrix. Formation of these vertically coupled quantum dot structures (VCQD's) is shown to result in a significant modification of electronic properties as compared to dots formed by a single-cycle InAs deposition.

II. EXPERIMENT

The samples studied in this work were grown by elemental source molecular-beam epitaxy (MBE) by using a Riber-32 MBE machine.[16] Growth rates were 0.8 μm/h for GaAs and 0.3 μm/h for InAs. Arsenic pressure was $2–3\times10^{-6}$ torr. After oxide desorption, a 0.5-μm-thick GaAs buffer was grown at 600 °C, then 200 Å of $Al_{0.3}Ga_{0.7}As$ was deposited, followed by a 20 Å/20 Å GaAs-$Al_{0.3}Ga_{0.7}As$ superlattice (five periods) and a 1000-Å GaAs layer. Then the substrate temperature was lowered to 480 °C and desired amounts of InAs and GaAs were deposited. Afterwards 100 Å of GaAs was grown at 480 °C, then the substrate temperature was increased to 600 °C and a 150-Å-thick GaAs layer was grown. This layer was followed by a 20 Å/20 Å GaAs-$Al_{0.3}Ga_{0.7}As$ superlattice (five periods) and

 © 1996 The American Physical Society

200 Å of $Al_{0.3}Ga_{0.7}As$; a 50-Å GaAs layer was grown on the top for surface protection. Reflection high-energy electron diffraction (RHEED) patterns were monitored during the growth. InAs was deposited by using a submonolayer [0.3 monolayer (ML)] deposition mode with 10-s growth interruptions introduced after each deposition cycle. Growth interruption after each GaAs deposition cycle equals 10 s. Formation of dots started after the deposition of a ~4.5-Å-thick InAs layer and led to the transformation of a streaky RHEED pattern to a dashed one. Further InAs deposition resulted in well-developed diffraction spots typical for a three-dimensional growth mode.

Transmission electron microscopy (TEM) studies were performed by using a high-voltage JEOL JEM1000 (1 MV) microscope. Calorimetric absorption spectroscopy[24] (CAS) was carried out at $T=500$ mK. The absorption due to the GaAs substrate has been subtracted from the CAS spectra.

III. FORMATION OF VERTICALLY COUPLED QUANTUM DOTS

A. Geometry

In Fig. 1 we show plan-view (a) and cross-section (d) TEM images of InAs VCQD's formed by three-cycle InAs-GaAs deposition. Average thickness of the InAs deposited in each cycle equals 5.5 Å. Each GaAs deposition cycle corresponds to an average thickness of 15 Å. As can be seen in Fig. 1(a), the average lateral size of the islands is close to 170±10 Å. The islands have a square base with main axes along [001] and [010]. The histograms of nearest-neighbor dot orientation [Figs. 1(b) and 1(c)] prove that the dots are arranged in a two-dimensional (2D) square lattice with primitive lattice vectors along the same directions. This ordering is clearly observed in all parts of the TEM image. Although the nature of lateral ordering can be much more complex than in the case of a single sheet of dots,[23] we believe it still has the same main reason,[17] i.e., repulsive interaction of strained islands via elastically anisotropic substrate. Each VCQD is composed of three vertically aligned parts separated by 2–4-ML-thick GaAs regions [see Fig. 1(d)]. The upper parts have a larger lateral size (~170 Å) than the lower part (~110 Å). The resulting arrangement of InAs insertions can be considered as an *artificial three-dimensional semiconductor crystal.*

Vertically correlated stacking of well-separated InAs islands in a GaAs matrix is reported in literature since 1985.[12,21] Recently stacking of very closely spaced islands has also been reported.[22] However, even in that case, the thickness of the GaAs separating layer was larger than the pyramid height by ~15 Å. In our case the height of the single pyramidlike island is ~50 Å.[18,19] The average thickness *of only 15 Å of GaAs* deposited is not sufficient to cover the InAs pyramid. Thus the deposition mode described here cannot be considered as simple vertically correlated stacking[12,21,22] and another explanation for the final arrangement is required.

B. Energetics of Stranski-Krastanow growth for InAs and GaAs deposition cycles

Single-cycle deposition of InAs on the GaAs (100) surface above the critical thickness (~4.5 Å) leads to the formation of pyramid-shaped InAs islands on the InAs wetting layer. The further growth of GaAs on a surface with wetting layer *and* locally formed islands is affected by the *inhomogeneous strain field* due to the pyramids.[25,20] The strain field modulates the surface chemical potential for Ga adatoms as follows (see, e.g., Ref. 25):

$$\mu^{\rm Ga}(\mathbf{r})=\left[\mu_0^{\rm Ga}+\frac{Y\epsilon_t^2(\mathbf{r})\Omega}{2}\right]+\gamma\Omega\kappa(\mathbf{r}). \qquad (1)$$

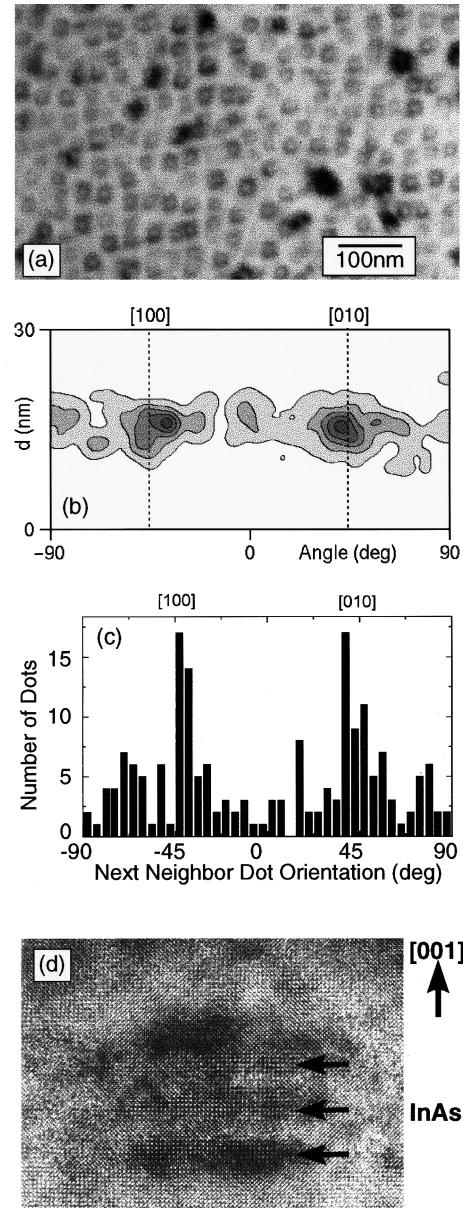

FIG. 1. Vertically coupled InAs quantum dots (VCQD's) in a GaAs matrix. (a) Bright-field plan-view transmission electron microscopy (TEM) micrograph under [100] zone axis illumination. (b) 2D histogram of two nearest neighbors' center to center distance and direction for the VCQD's from (a). (c) Projection of (b) onto the angular axis. Maxima in [100] and [010] directions prove VCQD arrangement on a 2D square lattice. (d) High-resolution electron microscopy [001] cross-section image formed by nine beams, defocusing is 60 nm; note the different spot density in InAs and GaAs regions.

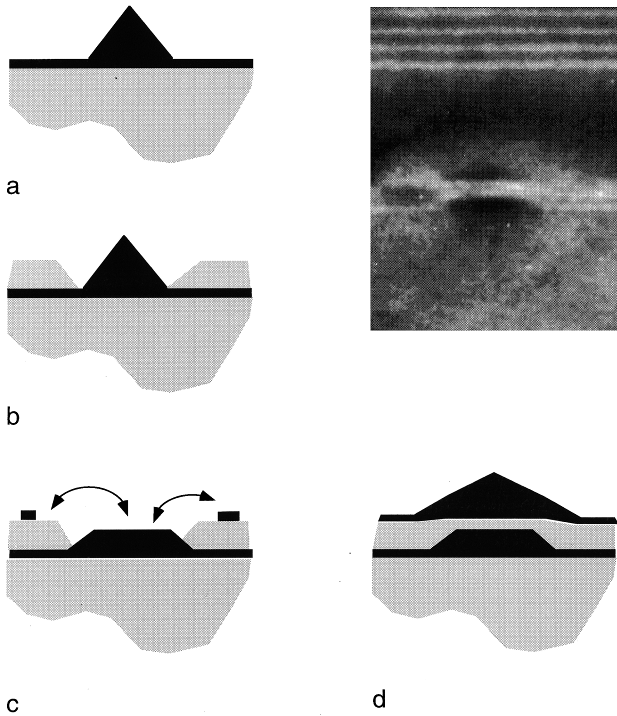

FIG. 2. (a)–(d) Schematic diagram of progressive stages of the formation of the coupled quantum dot structure. Efficient exchange reactions on the surface due to the energetics of Stranski-Krastanow growth occur during growth interruption on stage (c). Dark-field (g=400) [011] cross-section TEM image of the structure formed by 5-Å InAs–15-Å GaAs–5-Å InAs deposition is shown in the inset. The period of the upper AlAs-GaAs superlattice equals 40 Å.

Here μ_0^{Ga} is the chemical potential of Ga adatoms on the reference flat surface with the lattice parameter equal to that of the bulk GaAs. The second term in the square parentheses is the elastic energy correction to μ_0^{Ga}, where $\epsilon_t(\mathbf{r})$ is the tangential component of the local strain defined with respect to unstrained GaAs, Y is Young's modulus, and Ω is the atomic volume. The third term is the surface energy contribution to the chemical potential, where γ is the surface energy and $\kappa(\mathbf{r})$ is the local curvature of the surface. Due to the elastic energy correction to μ_0^{Ga}, the incorporation of GaAs on the facets of elastically relaxed InAs pyramids is energetically unfavorable. The gradient of the surface chemical potential leads to a locally directional migration of Ga adatoms away from the InAs islands [Figs. 2(a) and 2(b)]. The latter results in a reduction of the growth rate and in a curved growth front in the vicinity of the islands.[20] When the InAs islands are partly covered with GaAs, the effect of the strain inhomogeneity on the profile of the growing surface decreases, and the planar growth front is completely reestablished after the deposition of ~60 Å GaAs.[16,18,19]

The situation changes drastically if the GaAs growth is *interrupted well before the dots are completely covered with GaAs*, and another InAs deposition cycle is introduced (or just the growth interruption time is chosen to be long enough to let the system come to equilibrium). According to the SK InAs-GaAs growth mode, it is energetically favorable for InAs to evaporate from the InAs islands and to cover the free surface of GaAs, forming a second wetting layer. The surface chemical potential of In atoms is equal in this case to

$$\mu^{\mathrm{In}}(\mathbf{r})=\left[\mu_0^{\mathrm{In}}+\frac{Y[\epsilon_t(\mathbf{r})-\epsilon_0]^2\Omega}{2}\right]+\gamma\Omega\kappa(\mathbf{r})-\frac{\zeta\Omega\vartheta(\mathbf{r})}{a}. \quad (2)$$

Here μ_0^{In} is the chemical potential of In adatoms on the unstressed (completely relaxed) surface, where the lattice parameter is equal to that of InAs. The elastic energy correction is minimum for a completely relaxed surface, where $\epsilon_t(\mathbf{r})=\epsilon_0$ (ϵ_0 being the lattice mismatch between InAs and GaAs). The third term in Eq. (2) is the same as in Eq. (1). The last term represents the effect of wetting, where ζ is the energy benefit per unit area due to the formation of the wetting layer, a is the lattice parameter, and $\vartheta(\mathbf{r})=1$ on the GaAs surface and $\vartheta(\mathbf{r})=0$ on the InAs surface.

The last term in Eq. (2) plays the dominant role in the directed migration of indium atoms *before* the second wetting layer is formed. According to this term there exists a *thermodynamically favored tendency for indium atoms to be detached from the InAs island and to cover the free GaAs surface*. As the InAs pyramids are only partly covered with GaAs, the InAs of the upper part of the InAs island are available and the top of the pyramid can be completely dissolved at this stage. Since the second wetting layer is formed only partially, the directional migration of both In and Ga atoms is possible. Further evaporation of indium from the InAs pyramid will occur from the part laterally confined by GaAs unless the enhanced curvature of the nearby GaAs region, and, consequently, enhanced surface energy [last term in Eq. (1)] will make the planarization (partial or complete) of the GaAs surface by directional migration of Ga adatoms energetically more favorable. Then the rest of the InAs island will be completely confined by GaAs. Directional migration of Al and Ga adatoms was also found to result in spontaneous formation of the upper $\mathrm{Al}_x\mathrm{Ga}_{1-x}\mathrm{As}$ cladding on *flat* $\mathrm{In}_x\mathrm{Ga}_{1-x}\mathrm{As}$ islands during growth interruptions,[11] indicating that in the *2D case* (flat islands) this arrangement can also be *energetically* beneficial.[2]

Formation of split islands is possible only if the kinetics of surface exchange reactions is fast enough. After the GaAs is deposited, and the new InAs deposition cycle is just started, most of the surface is InAs-free, and the directed migration of In and Ga adatoms continues. At our substrate temperature (480 °C) and for the growth mode chosen (0.3-ML InAs deposition cycles with 10-s growth interruptions after each cycle) the kinetics is fast enough to produce severe morphological modifications even on a much larger geometrical scale.[19]

Simultaneously with the shape transformation of the InAs islands, the deposition of extra InAs occurs, finally resulting in a formation of a *complete* InAs wetting layer (~1.5 ML). Then, after the second wetting layer is formed, the second term in Eq. (2) provides the tendency for *excess* In atoms to attach to the region of locally modulated lattice parameter due to existing pyramid. According to this energy term the formation of InAs islands at *new* positions is energetically *unfavorable*. As a result, a vertical arrangement of two InAs islands separated by a several-monolayer-thick GaAs layer (split pyramid or VCQD) can be formed. Then the process can be continued. Schematically, the formation of the VCQD structure is illustrated in Figs. 2(a)–2(d).

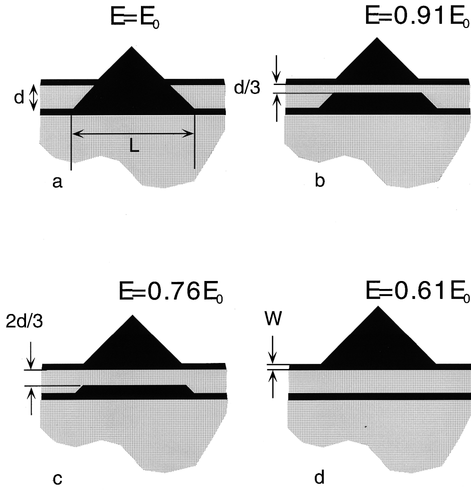

FIG. 3. (a)–(d) Schematic representation of several possible final states for multilayer InAs (black)–GaAs (gray) deposition. Relative dimensions used in calculations of the elastic energy are as follows: $d=3$ W, $L=24$ W. The tilt angle of the pyramid facets is 45°. We show that a reduction of the elastic energy for structures of (b)–(d) with respect to that of (a) occurs, caused by InAs transfer from the buried part to the uncovered part of the pyramid. No total energy reduction is induced by simple splitting without InAs transfer.

C. Strain energy of VCQD structures

The possibility to fabricate the VCQD structure depends also on the energetics of the split pyramid in respect to other possible arrangements. We compare the energetics of several possible final states. Figure 3(a) depicts the case where no splitting occurs. Figures 3(b)–3(d) refer to the situation where the buried part of the pyramid floats up partially [3(b), 3(c)] or completely [3(d)] and is replaced by GaAs. We estimate here the gain in the elastic energy for structures of Figs. 3(b)–3(d) with respect to that of Fig. 3(a). This gain is due to the fact that a certain volume of InAs is transferred from the buried region, where it is not relaxed, to the uncovered pyramid, where it is partially relaxed. The elastic energy for each of the structures of Fig. 3 is determined by

$$E_{\rm el}=\tfrac{1}{2}\lambda_{ijlm}^{(2)}\int_{(2)}[\epsilon_{ij}(\mathbf{r})-\epsilon_0\delta_{ij}][\epsilon_{lm}(\mathbf{r})-\epsilon_0\delta_{lm}]dV + \tfrac{1}{2}\lambda_{ijlm}^{(1)}\int_{(1)}\epsilon_{ij}(\mathbf{r})\epsilon_{lm}(\mathbf{r})dV. \quad (3)$$

Here indices (1) and (2) denote GaAs and InAs, respectively; λ_{ijlm} is the tensor of elastic moduli; $\epsilon_0=(a^{(2)}-a^{(1)})/a^{(1)}$ is the lattice mismatch; $\delta_{ij}=1$ if $i=j$, and $\delta_{ij}=0$ otherwise; $\epsilon_{ij}(\mathbf{r})$ is the strain tensor defined via the displacement vector $u_i(\mathbf{r})$ as follows:

$$\epsilon_{ij}(\mathbf{r})=\frac{1}{2}\left[\frac{\partial u_i(\mathbf{r})}{\partial r_j}+\frac{\partial u_j(\mathbf{r})}{\partial r_i}\right].$$

The displacement vector $u_i(\mathbf{r})$ in the heterophase system obeys equilibrium equations of the elasticity theory in each material,

$$\lambda_{ijlm}^{(1,2)}\frac{\partial^2 u_m(\mathbf{r})}{\partial r_j \partial r_l}=0 \quad (4)$$

obeys boundary conditions at the interface and at the free surface, and vanishes in the depth of the substrate. The boundary conditions at the InAs-GaAs interface read[1]

$$\lambda_{ijlm}^{(2)}n_j(\mathbf{r})\left[\frac{\partial u_m(\mathbf{r})}{\partial r_l}-\epsilon_0\delta_{lm}\right]\Bigg|^{(2)}=\lambda_{ijlm}^{(1)}n_j(\mathbf{r})\left[\frac{\partial u_m(\mathbf{r})}{\partial r_l}\right]\Bigg|^{(1)}, \quad (5a)$$

where $n(\mathbf{r})$ is the outer normal to the InAs region at the interface, and the boundary conditions at the free surface of InAs are as follows:[2]

$$\lambda_{ijlm}^{(2)}m_j(\mathbf{r})\left[\frac{\partial u_m(\mathbf{r})}{\partial r_l}-\epsilon_0\delta_{lm}\right]\Bigg|^{(2)}=0, \quad (5b)$$

where $m(\mathbf{r})$ is the outer normal to the free surface. We solve Eqs. (4) with the boundary conditions (5a) and (5b) by the finite element method, calculate the strain tensor $\epsilon_{ij}(\mathbf{r})$, evaluate the elastic energy from Eq. 3, subtract the elastic energy of the two wetting layers, and thus obtain the net *elastic energy* of each of the structures displaced in Fig. 3.

If we denote the net energy of the nonsplit pyramid of Fig. 3(a) as E_0, then the net energies of split pyramids are as follows: $0.89E_0$ for Fig. 3(b), $0.76E_0$ for Fig. 3(c), and $0.61E_0$ for Fig. 3(d). The energy gain per one transferred In atom equals, respectively, 42, 49, and 47 meV.

To analyze other possible shape transformations of the pyramid, we have calculated $E_{\rm el}$ for several split structures, where InAs from the buried part of the pyramid is transferred not to the uncovered part of the pyramid, but is redistributed between two planar wetting layers. Such a splitting *does not lead to a reduction of the elastic energy, but, to the contrary, results in the increase of the elastic energy* up to 1.20 E_0.

The cross-section TEM image of VCQD's formed by 5.5 Å InAs–15 Å GaAs–5.5 Å InAs deposition is shown in the inset of Fig. 2. Then the process can be repeated (see Fig. 1). The volume of each island progressively increases with successive deposition cycles of InAs due to the transfer of InAs from the buried part of the structure.

The theoretical analysis performed demonstrates that the elastic energy for structures like those of Figs. 3(b)–3(d) with respect to those of Fig. 3(a) is gained when at the final stage *a certain volume of InAs is transferred from the buried region where it is not relaxed to the uncovered pyramid where it is partially elastically relaxed*. This general conclusion is not affected by possible deviations of the real shape of islands from the simplified shapes of Fig. 3. Although the maximum energy gain would correspond to the complete transfer of the buried InAs to the uncovered part of the pyramid, the actual resulting shape of the island strongly depends on the kinetics of the growth process involved. Thus the *strain energy calculations also support the total energy reduction due to splitting of the pyramids, in addition to the energetics of the Stranski-Krastanow growth itself.* At the same time, for high deposition rates and low substrate temperatures, the splitting can be suppressed because of the slower kinetics of surface exchange reactions.

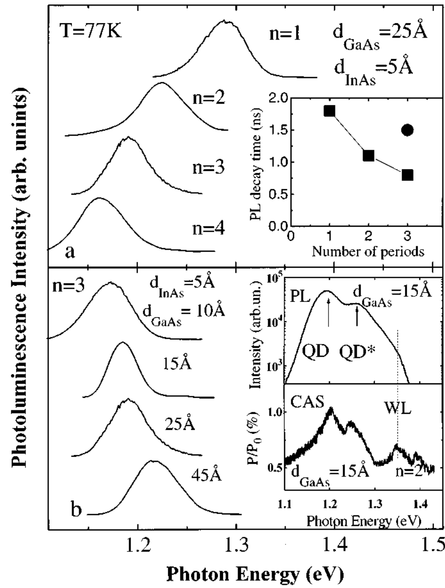

FIG. 4. Photoluminescence (PL) spectra of VCQD's grown with different number of InAs deposition cycles (a), and with different average thickness of the GaAs separating layer (b). The dependence of the PL decay time on the number of InAs deposition cycles for GaAs layer thickness (d_{GaAs}) of 15 Å is shown in the upper inset. Circle corresponds to a value obtained for d_{GaAs}=45 Å. A PL spectrum at high excitation density of ~500 W cm^{-2} and a calorimetric absorption spectrum (CAS) of the VCQD structure are shown in the lower inset.

IV. OPTICAL PROPERTIES OF VCQD's

The impact of the InAs-GaAs 2D-3D growth transition on the photoluminescence (PL) spectrum is the appearance of an intense [see, e.g., Fig. 4(a), upper curve] luminescence where the intensity maximum is strongly shifted towards smaller photon energies in comparison with the energy expected for the uniform InAs quantum well of the same average thickness.[12] This luminescence was attributed to radiative recombination of confined carriers in three-dimensional nanoscale islands, i.e., quantum dots.[12]

This conclusion was confirmed by results of photoluminescence,[13,15] time-resolved PL,[19] luminescence polarization,[19] and absorption[15] studies. Observation of ultrasharp luminescence lines due to single quantum dots which do not show broadening with temperature increase manifested the formation of *electronic* quantum dot.[16]

In Fig. 4 we show PL spectra of single-cycle quantum dots and of VCQD structures with the same separating GaAs average layer thickness (d_{GaAs}), but with different number of periods (a), and for the same number of periods ($n=3$), but with different d_{GaAs} (b). The PL decay time as a function of number of deposition cycles for the d_{GaAs}=15 Å case is shown in the inset of Fig. 4(a). A CAS spectrum and a PL spectrum at high excitation density are shown in the inset of Fig. 4(b). From the comparison of the PL spectrum and the CAS spectrum one can conclude that there is a pronounced absorption peak which *coincides in energy* with the main PL peak. For high excitation densities, additional peaks appear on the high-energy side of the PL spectrum. These features are marked ''QD*'' and ''WL'' and attributed to the excited state of the quantum dot exciton (QD*) and to the heavy hole exciton in the InAs wetting layers[16] (WL) coupled via the thin GaAs barrier, respectively. One can see that the increase in the number of InAs deposition cycles results in a shift of the PL line towards lower photon energies. Similar results have been recently observed in.[22] In the present work we also found similar behavior in the calorimetric absorption spectra. CAS are much less affected by the inhomogeneity of the system due to different shape of islands and different strain fields for dots in different stacks. The peak in the absorption spectrum corresponds to the *maximum in the density of states*, while in PL spectra it can correspond to the state with the lowest energy.

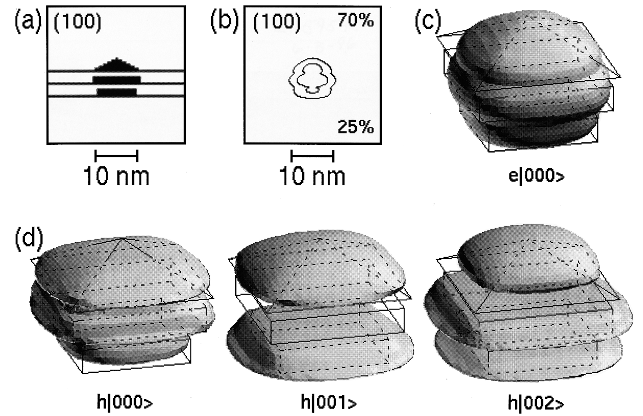

FIG. 5. Numerical simulation of coupled quantum dots: (a) geometry of the structure (i.e., In concentration), (b) (100) cross section of the contour plot for 25% and 70% of the ground-state electron wave-function orbital, (c) three-dimensional view of the ground-state electron wave function, and (d) three-dimensional view of ground and $|001\rangle$ and $|002\rangle$ excited hole states.

From Fig. 4 one can see that significant decoupling occurs with increase in d_{GaAs}, however, the PL peak energy does not approach the value characteristic for the single-cycle deposition even for d_{GaAs}=45 Å. Even more important is the PL decay time decrease with the increase in the number of InAs deposition cycles: 1.8, 1.1, and 0.8 ns for one, two, and three cycles, respectively. The exciton radiative lifetime in an isolated pyramidally shaped quantum dot is close to ~1.5 ns for dots in a relatively broad range of lateral sizes of ~80–120 Å and PL transition energies of ~1.3–1.1 eV, respectively.[19] If carriers were effectively confined in different InAs parts of VCQD structures and no wave-function overlap occurred, the observed lifetime decrease could not be explained by, e.g., variation of shape between each InAs part in the VCQD. Thus our results demonstrate an increase in the oscillator strength due to vertical coupling. The increase in the exciton oscillator strength can be explained on the basis of exciton coherence in symmetrically coupled quantum wells and dots.[26] The exciton coherence effect concentrates oscillator strength in the ground-state exciton.

V. ELECTRON AND HOLE LEVELS IN THE VCQD

To investigate the wave-function coherence across the split island we calculated the electronic states in the coupled quantum dots. In Fig. 5(a) we depict the assumed geometry

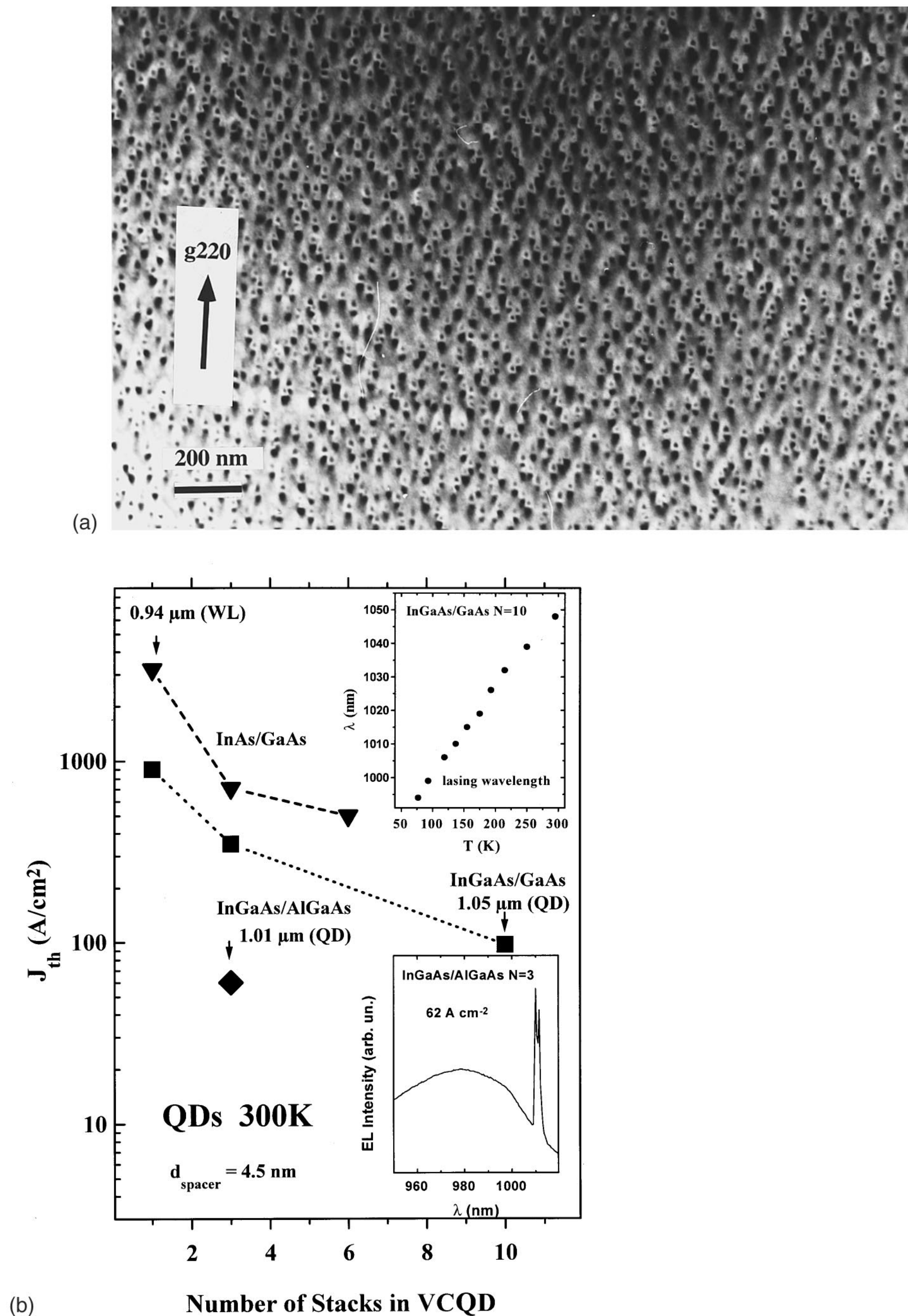

FIG. 6. (a) Typical plan-view transmission electron microscopy image of the $In_{0.5}Ga_{0.5}As/GaAs$ vertically coupled quantum dots. Average thickness of the $In_xGa_{1-x}As$ deposited per each cycle: 12 Å. Average thickness of the separating GaAs: 45 Å. Number of deposition cycles: 6. (b) Threshold current density vs number of periods in VCQD structure. Results for quantum dot lasers based on InAs/GaAs, $In_{0.5}Ga_{0.5}As/GaAs$, and $In_{0.5}Ga_{0.5}As/Al_{0.15}Ga_{0.85}As$ quantum dots are presented. Lasing wavelength vs temperature dependence is shown in the upper inset. Emission spectrum of the $In_xGa_{1-x}As/Al_xGa_{1-x}As$ VCQD laser at 300 K is presented in the lower inset.

of the three islands and the wetting layers. A numerical calculation of strain in the system of coupled islands is performed, using the same approach as described in Ref. 27. Subsequently the strained confinement potentials are calculated and then the three-dimensional Schrödinger equation is solved. We find that only one electron state is localized in the quantum dot; excited electron states largely extend into the wetting layers. In Fig. 5(b) contour plots for 25% and 70% of the ground-state electron wave-function orbital are shown together with a three-dimensional view [Fig. 5(c)]. It is clear that the wave function is coherent over the entire island stack. Spin-splitting effects[28] induced by the low symmetry of the system and resulting in split electron levels with spins up and down were not considered in the current calculations. Such effects will not affect the results qualitatively. For the holes we find several localized states due to their larger mass. Their wave functions are shown in Fig. 5(d). The first two excited hole states have their nodes in z direction and exhibit a separation from the ground state of 25 and 65 meV, respectively. In first-order perturbation theory the exciton binding energy in the threefold stack is 16 meV, i.e., comparable to the hole level separation. We expect therefore

strong Coulomb correlation which will lead to an increase of ground-state oscillator strength compared to uncoupled dots.

VI. INJECTION LASING IN VCQD STRUCTURES

The advantage of InAs-GaAs and $In_xGa_{1-x}As$-GaAs VCQD's is particularly important at high excitation densities and observation temperatures, when single deposition cycle dots (SQDs) and VCQD's were introduced in the active region of GaAs-$Al_xGa_{1-x}As$ double heterostructure lasers. The main objectives to use these structures are (i) to increase modal gain (possibly keeping the transparency current the same), (ii) to increase the quantum dot (QD) exciton oscillator strength (to decrease radiative lifetime), and (iii) to avoid thermal depopulation of QDs by increasing the relative density of QD-induced states compared to GaAs matrix-induced states (to maintain QD exciton lasing up to room temperature).

As was shown in Ref. 29, the introduction of a dense two-dimensional array of quantum dots in the active region of a GaAs-$Al_xGa_{1-x}As$ double heterostructure laser allows realization of lasing via the ground state of QDs at low temperatures. Lasing was found to occur near the maximum of the quantum dot PL spectrum recorded at low excitation densities, and the threshold current was found to be practically temperature insensitive in a wide temperature range up to ~80 K for InAs QDs and up to 150 K for $In_xGa_{1-x}As$ QDs in agreement with theoretical predictions.[30,31] At the same time, at elevated temperatures, thermal evaporation of carriers from QDs resulted in a strong decrease in the QD related gain for constant injection current, and, thus, in a remarkable increase in the threshold current density. The lasing energy was close to one corresponding to the wetting layer heavy hole exciton energy at 300 K.[19]

In this work the laser structure geometry is kept essentially the same as in Refs. 19 and 29, but VCQD's (Refs. 32–34) are introduced in the active region. In Fig. 6(b) we demonstrate the influence of the number of periods (N) in VCQD structure on the threshold current density at 300 K for $In_xGa_{1-x}As$ and InAs VCQD's in a GaAs matrix, and for $In_{0.5}Ga_{0.5}As$ VCQD's in an $Al_{0.15}Ga_{0.85}As$ matrix. The thickness of the separating GaAs or $Al_xGa_{1-x}As$ layer is 45 Å. The average thickness of the InAs deposited in each cycle equals 5 Å for the InAs/GaAs VCQD's, and the average thickness of the $In_xGa_{1-x}As$ deposited equals 12 Å for the $In_xGa_{1-x}As$-GaAs and $In_xGa_{1-x}As$-$Al_xGa_{1-x}As$ VCQD's. A typical strong-beam plan-view TEM image of the $In_xGa_{1-x}As$/GaAs VCQD structure is shown in Fig. 6(a). One can conclude that increase in N results in a marked decrease in the threshold current density down to 90 A/cm^2 for $In_{0.5}Ga_{0.5}As$-GaAs VCQD's ($N=10$) and down to 60 A/cm^2 for $In_{0.5}Ga_{0.5}As$-$Al_{0.15}Ga_{0.85}As$ VCQD's ($N=3$) for samples with four cleaved facets (totally internally reflecting structures). For stripe lasers ($L=1.5$–2 mm) the threshold current density is typically 20–40 % higher. The emission spectrum at 62 A/cm^2 of the $In_xGa_{1-x}As$-$Al_xGa_{1-x}As$ VCQD laser is shown in the lower inset of Fig. 6. The improved value of the threshold current density (J_{th}) for the $Al_xGa_{1-x}As$-$In_xGa_{1-x}As$ VCQD structure is attributed to a much larger energy separation between the quantum dot and the wetting layer states preventing the thermal evaporation of carriers.

Increase in N for InAs dots from 1 to 3 results in a moderate extension of the high-temperature stability range from 80 to 180 K. The characteristic temperature (T_0) in this range equals 350–420 K. For $In_xGa_{1-x}As$ dots no increase of the high T_0 range of 20–180 K was observed up to $N=3$. Further increase in N results in a decrease of the high T_0 stability range to about 140 K both for InAs and $In_xGa_{1-x}As$ dots. The threshold current density measured in this range decreases with increasing N from about 80 A cm^{-2} for $N=1$ down to 15 A cm^{-2} (120 K, $N=10$). The most remarkable difference between structures with small and large N is the increase in T_0 value in the vicinity of 300 K. T_0 near 300 K increases from 60 ($N=1$, 3) to 150 K for $N=10$. For large N the lasing energy follows the GaAs band-gap dependence on temperature rise, as is shown in the upper inset of Fig. 6. For $N \geqslant 3$ the lasing energy coincides with the ground-state QD exciton transition energy revealed in PL spectra at all temperatures, as was also reported in Ref. 32.

VII. CONCLUSION

To conclude, we have observed a spontaneous island shape transformation effect in Stranski-Krastanow growth which permits fabrication of a three-dimensional tetragonal lattice of very strongly vertically coupled quantum dots. The energetics of the Stranski-Krastanow growth mode and the reduction of strain energy of the final state govern the observed mass transfer of InAs from the lower to the upper part of the coupled quantum dot structure. We demonstrate that the dots are also electronically coupled in the vertical direction and that their properties are significantly modified. In particular, a decrease of the radiative lifetime is observed. We demonstrate that VCQD arrays are decisive for reducing the threshold current density and increasing the temperature stability of QD lasers.

ACKNOWLEDGMENTS

Parts of this work are supported by the Volkswagen Stiftung, by INTAS, Grant No. INTAS-94-1028, and by Deutsche Forschungsgemeinschaft in the framework of Sfb. 296 N.N.L. thanks the Alexander von Humboldt Foundation.

*On leave from A. F. Ioffe Physical-Technical Institute, St. Petersburg, Russia.

[1] A. G. Khachaturyan, *Theory of Structural Transformations in Solids* (Wiley, New York, 1983).

[2] I. P. Ipatova, V. G. Malyshkin, and V. A. Shchukin, J. Appl. Phys. **74**, 7198 (1993); Philos. Mag. B **70**, 557 (1994).

[3] R. Nötzel, N. N. Ledentsov, L. Däweritz, M. Hohenstein, and K. Ploog, Phys. Rev. Lett. **67**, 3812 (1991).

[4] R. Koch, M. Borbonus, O. Haase, and K. H. Rieder, Phys. Rev. Lett. **67**, 3416 (1991).

[5] V. I. Marchenko, Zh. Eksp. Teor. Fiz. **81**, 1141 (1981) [Sov. Phys. JETP **54**, 605 (1981)].

[6] V. A. Shchukin, A. I. Borovkov, N. N. Ledentsov, and P. S. Kop'ev, Phys. Rev. B **51**, 10 104 (1995); V. A. Shchukin, A. I.

Borovkov, N. N. Ledentsov, and D. Bimberg, *ibid*. **51**, 17 767 (1995).
[7] V. I. Marchenko, Pis'ma Zh. Eksp. Teor. Fiz. **33**, 397 (1981) [JETP Lett. **33**, 381 (1981)].
[8] J. Tersoff and R. M. Tromp, Phys. Rev. Lett. **70**, 2782 (1993).
[9] V. Bressler-Hill, A. Lorke, S. Varma, P. M. Petroff, K. Pond, and W. H. Weinberg, Phys. Rev. B **50**, 8479 (1994).
[10] P. D. Wang, N. N. Ledentsov, C. M. Sotomayor Torres, P. S. Kop'ev, and V. M. Ustinov, Appl. Phys. Lett. **64**, 1526 (1994).
[11] R. Nötzel, J. Temmyo, and T. Tammamura, Nature (London) **369**, 131 (1994).
[12] L. Goldstein, F. Glas, J. Y. Marzin, M. N. Charasse, and G. Le Roux, Appl. Phys. Lett. **47**, 1099 (1985).
[13] D. Leonard, M. Krishnamurthy, C. M. Reaves, S. P. Denbaars, and P. M. Petroff, Appl. Phys. Lett. **63**, 3203 (1993).
[14] J. M. Moison, F. Houzay, F. Barthe, L. Leprice, E. Andre, and O. Vatel, Appl. Phys. Lett. **64**, 196 (1994).
[15] N. N. Ledentsov, M. Grundmann, N. Kirstaedter, J. Christen, R. Heitz, J. Böhrer, F. Heinrichsdorff, D. Bimberg, S. S. Ruvimov, P. Werner, U. Richter, U. Gösele, J. Heydenreich, V. M. Ustinov, A. Yu. Egorov, M. V. Maximov, P. S. Kop'ev, and Zh. I. Alferov, in *Proceedings of the 22nd International Conference on the Physics of Semiconductors, Vancouver, 1994*, edited by D. J. Lockwood (World Scientific, Singapore, 1995), Vol. 3, p. 1855.
[16] M. Grundmann, J. Christen, N. N. Ledentsov, J. Böhrer, D. Bimberg, S. S. Ruvimov, P. Werner, U. Richter, U. Gösele, J. Heydenreich, V. M. Ustinov, A. Yu. Egorov, A. E. Zhukov, P. S. Kop'ev, and Zh. I. Alferov, Phys. Rev. Lett. **74**, 4043 (1995).
[17] V. A. Shchukin, N. N. Ledentsov, P. S. Kop'ev, and D. Bimberg, Phys. Rev. Lett. **75**, 2968 (1995); V. A. Shchukin, N. N. Ledentsov, M. Grundmann, P. S. Kop'ev, and D. Bimberg, Surf. Sci. **352-354**, 117 (1996).
[18] S. S. Ruvimov, P. Werner, K. Scheerschmidt, U. Richter, U. Gösele, J. Heydenreich, N. N. Ledentsov, M. Grundmann, D. Bimberg, V. M. Ustinov, A. Yu. Egorov, P. S. Kop'ev, and Zh. I. Alferov, Phys. Rev. B **51**, 14 766 (1995).
[19] N. N. Ledentsov, M. Grundmann, N. Kirstaedter, O. Schmidt, R. Heitz, J. Böhrer, D. Bimberg, V. M. Ustinov, V. A. Shchukin, P. S. Kop'ev, Zh. I. Alferov, S. S. Ruvimov, A. O. Kosogov, P. Werner, U. Richter, U. Gösele, and J. Heydenreich, Solid-State Electron. **40**, 785 (1996).
[20] Q. Xie, P. Chen, and A. Madhukar, Appl. Phys. Lett. **65**, 2051 (1994).
[21] Q. Xie, A. Madhukar, P. Chen, and N. Kobayashi, Phys. Rev. Lett. **75**, 2542 (1995).
[22] G. S. Solomon, J. A. Trezza, A. F. Marshall, and J. S. Harris, Jr., Phys. Rev. Lett. **76**, 952 (1996).
[23] J. Tersoff, C. Teichert, and M. Lagally, Phys. Rev. Lett. **76**, 1675 (1996).
[24] A. Juhl and D. Bimberg, J. Appl. Phys. **64**, 303 (1988).
[25] D. J. Srolovitz, Acta Metall. **37**, 621 (1989).
[26] G. W. Bryant, Phys. Rev. B **47**, 1683 (1993).
[27] M. Grundmann, O. Stier, and D. Bimberg, Phys. Rev. B **51**, 11 969 (1995).
[28] P. Pfeffer and W. Zawadzki, Phys. Rev. B **52**, R14 332 (1995).
[29] N. Kirstaedter, N. N. Ledentsov, M. Grundmann, D. Bimberg, U. Richter, S. S. Ruvimov, P. Werner, J. Heydenreich, V. M. Ustinov, M. V. Maximov, P. S. Kop'ev, and Zh. I. Alferov, Electron. Lett. **30**, 1416 (1994).
[30] Y. Arakawa and H. Sakaki, Appl. Phys. Lett. **40**, 939 (1982).
[31] M. Asada, Y. Miyamoto, and Y. Suematsu, IEEE J. Quantum Electron. **22**, 1915 (1995).
[32] Zh. I. Alferov, N. A. Bert, A. Yu. Egorov, A. E. Zhukov, P. S. Kop'ev, I. L. Krestnikov, N. N. Ledentsov, A. V. Lunev, M. V. Maximov, A. V. Sakharov, V. M. Ustinov, A. F. Tsatsulnikov, Yu. M. Shernyakov, and D. Bimberg, Fiz. Tekh. Poluprovodn. **30**, 351 (1996) [Semiconductors **30**, 194 (1996)].
[33] D. Bimberg, N. N. Ledentsov, M. Grundmann, N. Kirstaedter, O. G. Schmidt, M. H. Mao, V. M. Ustinov, A. Yu. Egorov, A. E. Zhukov, P. S. Kop'ev, Zh. I. Alferov, S. S. Ruvimov, U. Gösele, and J. Heydenreich, Phys. Status Solidi B **194**, 159 (1996).
[34] N. N. Ledentsov, J. Böhrer, D. Bimberg, S. V. Zaitsev, V. M. Ustinov, A. Yu. Egorov, A. E. Zhukov, M. V. Maximov, P. S. Kop'ev, Zh. I. Alferov, A. O. Kosogov, U. Gösele, and S. S. Ruvimov, in Proceedings of the Spring Meeting of the Materials Research Society, April 8–12 1996, San Francisco, 1996 (Materials Research Society, Pittsburgh, in press).